

# The AUV design based on component modeling and simulation

Azadeh Kebriaee\*<sup>1</sup> and Hamidreza Nasiri<sup>2</sup>

<sup>1</sup>Mechanical Engineering school, Sharif University of Technology, Tehran, Iran

<sup>2</sup>Electrical Engineering school, Sharif University of Technology, Tehran, Iran

(Received October 4, 2011, Revised March 15, 2012, Accepted April 15, 2012)

**Abstract.** In the present work, design procedure and computer simulation of an *AUV* are documented briefly. The design procedure containing the design of propulsion system and *CFD* simulation of hydrodynamics behavior of the hull leads to achieve an optimum mechanical performance of *AUV* system. After designing, a comprehensive one dimensional model including motor, propeller, and *AUV* hull behavior simulates the whole dynamics of *AUV* system. In this design, to select the optimum *AUV* hull, several noses and tails are examined by *CFD* tools and the brushless motor is selected based on the first order model of *DC* electrical motor. By calculating thrust and velocity in functional point, OpenProp as a tool to select the optimum propeller is applied and the characteristics of appropriate propeller are determined. Finally, a computer program is developed to simulate the interaction between different components of *AUV*. The simulation leads to determine the initial acceleration, final velocity, and angular velocity of electrical motor and propeller. Results show the final *AUV* performance point is in the maximum efficiency regions of *DC* electrical motor and propeller.

**Keywords:** autonomous underwater vehicle; optimum design; contra-rotating propeller; computer simulation

---

## 1. Introduction

*AUVs* (*autonomous underwater vehicle*) are marine vehicles using no direct operator from the control station. The *AUV* is widely applied in providing the map of discovery zone and selecting the optimum place to install undersea structure in the oil and gas discovery, detecting the mine zones or undersea vehicles in the forbidden region in the military missions, and studying the components of ocean floor. In the optimum design of *AUV*, the main attention has been devoted to achieve the most efficient bare hull with minimum resistance drag. De Barros et al. presented a comparative study of *CFD* and *ASE* methods to predict the normal force and moment coefficients of the *AUV*. They used a 2-D axisymmetric body as the *AUV* hull to simulate the hydrodynamic behaviour by Fluent 6.2, using the *k- $\omega$*  shear stress transport for turbulence model (De Barros et al. 2008). In addition, Bertam and Alvarez discussed about different aspects to optimize the *AUV* hull (Bertram and Alvarez 2006). Lutz and Wagner applied numerical tool to optimize the shape of axisymmetric *NLF* bodies. The main objective of the optimization was based on minimization of the volumetric drag coefficient for different Reynolds numbers with no geometric constraints, (Lutz and Wagner 1998).

---

\*Corresponding author, Ph. D., E-mail: [Kebriaee@mech.sharif.ir](mailto:Kebriaee@mech.sharif.ir)

Alvarez *et al.* also investigated the optimum hull shape of an underwater vehicle moving near the free surface. They applied a first-order Rankin panel method to compute the wave resistance on an axisymmetric body moving close to the free surface. An annealing algorithm was utilized to search the hull parameters that minimize the wave resistance (Alvarez *et al.* 2009). Joung *et al.* studied on the design of an *AUV* to minimize drag force by using *CFD* analysis. Their *CFD* model consisted of *AUV* hull with a ducted propeller and the optimization algorithm was based on searching and identifying optimum design variables to produce minimum resistance (Joung *et al.* 2009). Phillips *et al.* proposed four key stages as the design of the hull fairing and control surfaces, calculation of *AUV* propulsive power (resistance and propulsion), and estimation of the dynamic stability and maneuverability to optimum the *AUV* hull by utilizing a *CFD* package, (Phillips *et al.* 2010).

But there are few studies on the design of *AUV* propulsion systems. OpenProp, an open source, was developed to design the most optimum fully-submerged propeller specifically for *AUV* in Massachusetts Institute of Technology (Epps 2010).

The total optimization in design of ship, *AUV*, and submarine was also studied at Virginia Tech Aerospace and Ocean Engineering Department for several years, (Brown and Thomas 1998, Chen 1999, Good and Brown 2006, Alemayehu *et al.* 2006, Martz 2008). Traditionally, procedure of *AUV* design has been largely based on experience and rules of thumb. Martz developed a Multiple Objective Genetic Optimization (*MOGO*) algorithm. The genetic algorithm searched the design space for optimal, feasible designs by considering cost, risk and effectiveness, (Shome *et al.* 2008). Shome *et al.* described the design aspects of an *AUV* including the detail mechanical design, software architecture, controllers and integration of various sensors. They also discussed about the simulation results in the preliminary trial of the system, (Mackay 2003).

In this work, a comprehensive detail design is developed to consider different components of *AUV* system involving *AUV* hull, propeller design, and selection of *DC* electrical motor. Finally, the dynamics behavior of *AUV* system is simulated based on the modeling of every element.

## 2. Solution methodology

Before designing, the constraints as well as the targets should be defined: The hull constraint is on the length being less than 100 centimeters. In addition, the power of propulsion system should be provided with a 6-cell pack of Lithium-Polymer battery with 5000 mAh energy, 3.7 V, and 30 C nominal max. rate. The final target is to reach the maximum velocity in the straight path.

The mechanical design of an *AUV* includes designing the hull and propulsion system involving motor and propeller.

The first part of *AUV* design is related to select the best hull. The bare hull with minimum drag in a wide range of functional velocity is the best choice to obtain the desired purpose. In the present work, some famous hulls (Shome *et al.* 2008, Joubert 2006, Michel 1951) are examined to select the best one by using the *CFD* tools.

The propeller design is the second step in the mechanical design of *AUV*. Single propellers (*SP*) are the popular propulsions to drive low velocity *AUVs*. Since the rotation torque of *SP* causes to heel in high velocity fully submerged body, the contra-rotating propeller (*CRP*) should be utilized to omit the torque in *AUV*. The *CRP* contains two propellers rotating in the opposite direction to cancel the torque of each other. The efficiency of *CRP* is more than single propeller due to the interaction velocity induced on the blade of propellers. In addition, embedding a duct around the

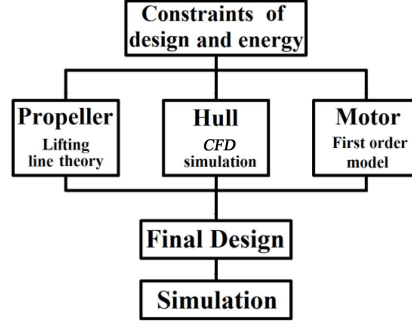


Fig. 1 the procedure of optimum mechanical design of AUV

propellers leads to increase the thrust in low AUV velocity and reduce the noise of propeller. In the present work, the lattice vortex lifting line theory is applied to design ducted contra-rotating propeller (DCRP). The lattice vortex lifting line theory designs the optimum geometry of the propeller for certain diameters, speed rotations, and blade numbers. To reduce the computational time of propeller design, the genetic algorithm coupled with artificial neural network is applied to select the optimum DCRP.

Then, brushless electrical motors should be utilized in the AUV propulsion to get more efficiency. The first order model is applied to compare different DC electrical motors for consistency with AUV hull and DCRP. The angular velocity of motor is determined by DCRP performance and motor power is limited by battery power.

Finally, the dynamic behavior of AUV is simulated to evaluate the procedure of design. Fig. 1 illustrates different parts of mechanical design of AUV schematically.

### 3. The design of AUV hull

The internal arrangement of AUV dictates that the diameter of AUV should be at least 15 centimeters. So the maximum of *length to diameter ratio* (LDR) of AUV is about 6.6 categorized in the short set of AUV.

The common shape of AUV hull contains three fundamental parts: nose, tail and mid part. The nose shape can effect essentially on the AUV hull in the downstream of flow and disturb the flow. It also effects on the performance of sonar system embedding in the AUV nose. The mid part has a parallel shape linking the nose and tail parts. The tail profile also effects on drag by changing the separation point position due to adverse pressure gradient.

Though applying the inverse method is the best procedure to find the optimum profile of the AUV hull, the comparison between different options of nose and tails are utilized to select the best hull in this paper. Table 1 introduces different shapes of AUV hull. An axisymmetric computational domain is applied to select the best bare hull. The continuity and axisymmetric Reynolds average Navier-Stokes equations (RANS) to find the velocity components  $\bar{\mathbf{u}} = (u_r, u_z)$  in cylindrical coordinate  $(r, z)$  can be expressed as

$$\frac{1}{r} \frac{\partial \rho r u_r}{\partial r} + \frac{\partial \rho u_z}{\partial z} = 0 \quad (1)$$

Table 1 Calculated drag force of different hulls

	Nose	Tail	drag (N)
1	Joubert (2006)	Joubert (2006)	56.840
2	NACA0015	Joubert (2006)	50.549
3	NACA0014 (Michel (1951))	Joubert (2006)	50.155
4	Shome <i>et al.</i> (2008)	Joubert (2006)	50.340
5	Shome <i>et al.</i> (2008)	Joubert (2006)	50.725

$$\frac{\partial \rho r u_r u_r}{\partial r} + \frac{\partial \rho r u_z u_r}{\partial z} = -r \frac{\partial p}{\partial r} + \frac{\partial}{\partial r} \left( \mu r \frac{\partial u_r}{\partial r} \right) + \frac{\partial}{\partial z} \left( \mu r \frac{\partial u_r}{\partial z} \right) + S_{u_r} \quad (2)$$

$$\frac{\partial \rho r u_r u_z}{\partial r} + \frac{\partial \rho r u_z u_z}{\partial z} = -r \frac{\partial p}{\partial z} + \frac{\partial}{\partial r} \left( \mu r \frac{\partial u_z}{\partial r} \right) + \frac{\partial}{\partial z} \left( \mu r \frac{\partial u_z}{\partial z} \right) + S_{u_z} \quad (3)$$

where  $p$ ,  $\rho$ , and  $\mu$  are the equilibrium pressure, density and viscosity coefficient, respectively.  $S_{u_r}$ ,  $S_{u_z}$  are also defined as the turbulent source terms

$$S_{u_r} = \rho \overline{u'_\theta u'_\theta} - \frac{\partial}{\partial r} (r \rho \overline{u'_r u'_r}) - \frac{\partial}{\partial z} (r \rho \overline{u'_z u'_r}) \quad (4)$$

$$S_{u_z} = -\frac{\partial}{\partial r} (r \rho \overline{u'_r u'_z}) - \frac{\partial}{\partial z} (r \rho \overline{u'_z u'_z}) \quad (5)$$

Based on Boussinesq's hypothesis, the turbulent Reynolds stresses are defined as follows

$$-\rho \overline{u'_j u'_j} = \mu_t \left( \frac{\partial u_j}{\partial x_j} + \frac{\partial u_j}{\partial x_j} \right) - \frac{2}{3} \left( \rho k + \mu_t \frac{\partial u_i}{\partial x_i} \right) \delta_{ij} \quad (6)$$

The  $k$ - $\varepsilon$  model is applied to model turbulent flow.  $k$  and  $\varepsilon$  are turbulent kinetic energy and turbulent dissipation rate respectively and  $\mu_t$  is the turbulent eddy viscosity

$$\mu_t = \rho C_\mu \frac{k^2}{\varepsilon} \quad (7)$$

The  $k$ - $\varepsilon$  equations are defined by

$$\frac{\partial \rho r k u_r}{\partial r} + \frac{\partial \rho r k u_z}{\partial z} = -\rho \varepsilon + G_k + \frac{\partial}{\partial r} \left( \left( \mu + \frac{\mu_t}{\sigma_k} \right) r \frac{\partial k}{\partial r} \right) + \frac{\partial}{\partial z} \left( \left( \mu + \frac{\mu_t}{\sigma_k} \right) r \frac{\partial k}{\partial z} \right) \quad (8)$$

$$\frac{\partial \rho r \varepsilon u_r}{\partial r} + \frac{\partial \rho r \varepsilon u_z}{\partial z} = -\rho \varepsilon + C_{1\varepsilon} \frac{\varepsilon}{K} G_k - C_{2\varepsilon} \rho \frac{\varepsilon^2}{K} + \frac{\partial}{\partial r} \left( \left( \mu + \frac{\mu_t}{\sigma_\varepsilon} \right) r \frac{\partial \varepsilon}{\partial r} \right) + \frac{\partial}{\partial z} \left( \left( \mu + \frac{\mu_t}{\sigma_\varepsilon} \right) r \frac{\partial \varepsilon}{\partial z} \right) \quad (9)$$

where  $G_k$  is the generation of turbulence kinetic energy due to the mean velocity gradients

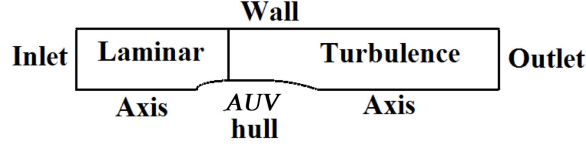


Fig. 2 Computational domain of AUV hull

$$G_k = -\overline{\rho u_j' u_j'} \frac{\partial u_i}{\partial X_j} \quad (10)$$

In addition, invariables in Eqs. (7)-(9) are introduced as follows

$$C_{1\varepsilon} = 1.44, \quad C_{2\varepsilon} = 1.92, \quad C_\mu = 0.09, \quad \sigma_k = 1.0, \quad \sigma_\varepsilon = 1.3 \quad (11)$$

Fig. 2 depicts the boundary conditions are defined as the velocity constant in the inlet, zero normal gradients of velocity components in the outlet, and no shear stress wall on the top, respectively. Based on critical Reynolds number ( $Re_X = u_\infty X/\nu = 2 \times 10^6$ ) in external flow, there is a predictable transient point from laminar to turbulent flow along the length of the hull. To study more accurately behavior flow on the bare hull, the computational domain is divided to laminar and turbulent regions. One of the robust criteria to calculate the transient point is the critical Reynolds number defined by characteristic length of  $\theta$ .  $\theta$  is the momentum thickness of boundary layer calculated by

$$\theta = \int_0^\infty \frac{u}{u_\infty} \left(1 - \frac{u}{u_\infty}\right) dy \quad (12)$$

where  $u_\infty$  is the velocity in the edge of boundary layer and  $y$  is the distance from the wall. After calculating the  $Re_\theta$  along the hull length, the transition point is determined at the point satisfying in the following equation, (Keller 1966).

$$Re_{\theta_{critical}} = 1.174 \left(1 + \frac{22400}{Re_X}\right) Re_X^{0.46} \quad (13)$$

As mentioned, OpenFOAM, CFD tool, is applied to solve the flow field around the hull. An

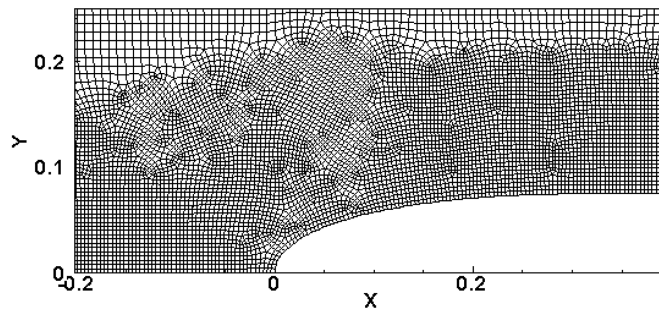


Fig. 3 Refined mesh near nose and boundary layer

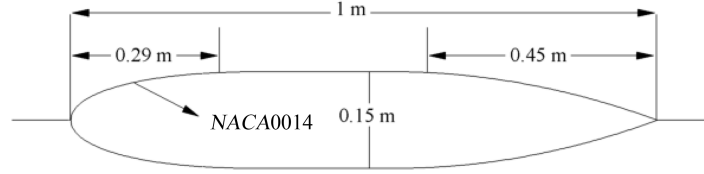


Fig. 4 The final optimal AUV hull

unstructured tetrahedral axisymmetric mesh is defined as the computational domain. Fig. 3 presents refined mesh near the AUV hull nose and across the boundary layer. Eqs. (1)-(3) and (8)-(9) are integrated numerically based on finite volume method to determine drag on the bare hull. The SIMPLE algorithm is also applied to couple pressure-velocity field in Navier-Stoke equations.

According to available battery power and a thumb calculation, the velocity of 8 m/s is predicted for the AUV. Table 1 presents the results of CFD simulation for different hull shapes in the velocity of 8 m/s. Comparing the hulls of (4) and (5) shows the tail suggested in (Michel 1951) has less undesired effect on AUV hull drag. Also comparing (1-4) cases of table 1 points out AUV hull with NACA0014 nose shape has the minimum drag compared to the other cases. So the hull shape is finalized with NACA0014 and the tail with following equation as the best AUV hull (Michel 1951)

$$\frac{r}{D} = \frac{1}{3}\left(\frac{X_A}{D}\right) - \frac{1}{18}\left(\frac{X_A}{D}\right)^2 \quad (14)$$

where  $r$  is the hull radius in each cross section,  $X_A$  is the distance length from the tail hull and  $D$  is the maximum diameter of AUV hull. The geometry of the best hull with the NACA0014 nose is shown in Fig. 4. In addition, Fig. 5 illustrates the pressure distribution around the nose and tail for hull velocity of 8 m/s. A stagnation point is predicted near the nose as well as a weaker one near the tail. Fig. 6 also presents velocity distribution around the hull for  $v = 8$  m/s. As seen, the velocity distribution has no disturbance or vortex near the hull. The boundary layer can be detected along the AUV hull and a thin wake has also been pushed after the hull tail.

Figs. 7 and 8 point out the turbulent kinetic energy  $k$  and turbulent dissipation rate  $\varepsilon$  for  $v = 8$  m/s, respectively. The turbulent kinetic energy and dissipation rate can be just seen after 20% of hull length in the turbulent regime. The gradient of velocity components across the boundary layer leads to generate the turbulent regime, while the rest of flow behaves as laminar flow with no turbulent

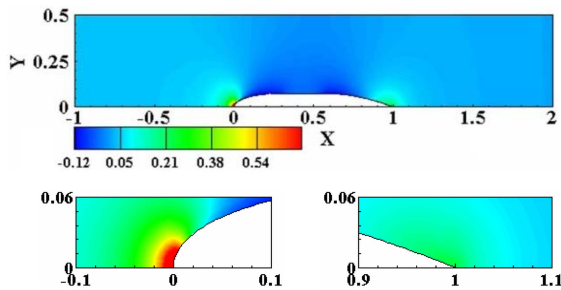


Fig. 5 Pressure distribution around the hull (Right: near the nose, Left: near the tail)

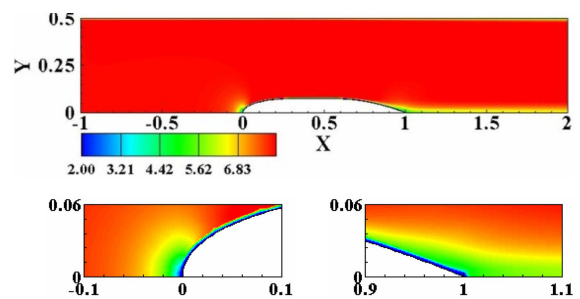


Fig. 6 Velocity distribution around the hull (Right: near the nose, Left: near the tail)

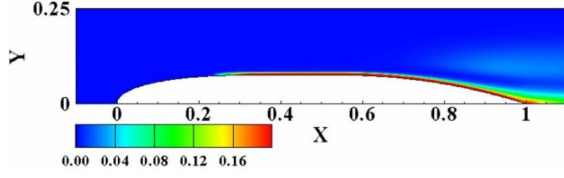


Fig. 7 Turbulent kinetic energy distribution around the hull

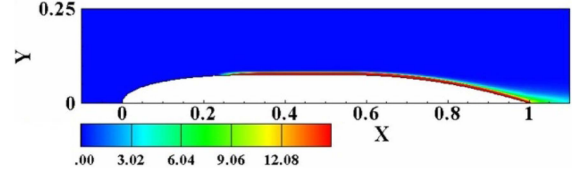


Fig. 8 Dissipation rate around the hull

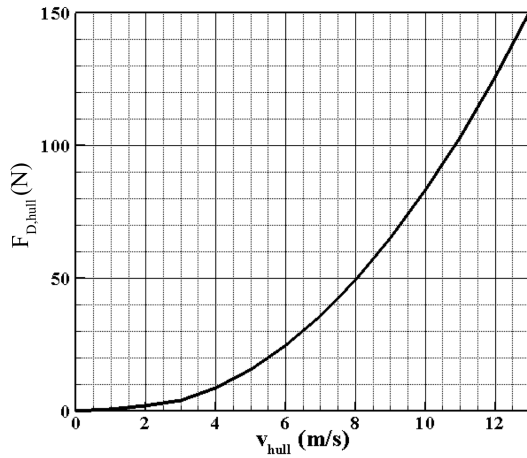


Fig. 9 The hull drag vs. velocity

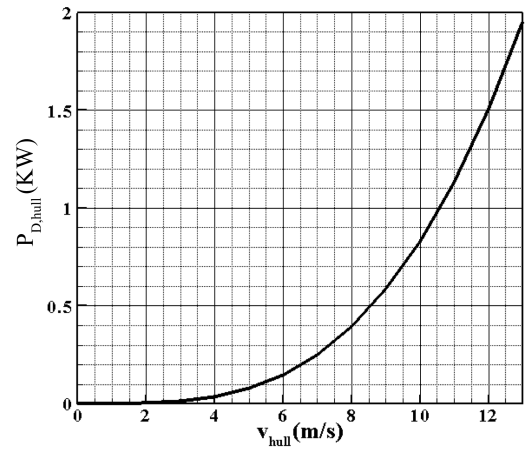


Fig. 10 The required power vs. velocity

characteristics. Besides, the wake behind of the hull generate turbulent characteristics after  $x = 1$  m. After selecting the best hull, *CFD* tool is applied to calculate resistance force for the velocity between the ranges of 1-15 m/s for the best bare hull. Mesh independency shows 50000 volume cells are sufficient to simulate flow field. Besides, an algebraic equation is applied to consider the effect of appendage drag force  $F_{D, app}$  as follows (Alemayehu 2006).

$$F_{D, app} = \frac{\rho}{2} V_{hull}^2 (A_{app} CD_{app} + App) \quad (15)$$

where  $V_{hull}$  is the hull velocity,  $A_{app} = 0.028 \text{ m}^2$  is the total area of appendage,  $CD_{app} = 0.009$  is the drag coefficient of appendage, and  $App$  is the empirical constant to consider the effect of other appendages i.e., sensors defined as (Alemayehu 2006)

$$App = \frac{L_{hull} D_{hull}}{1000} \quad (16)$$

$L_{hull}$  and  $D_{hull}$  are the length and maximum diameter of the *AUV* hull, respectively.

Finally Fig. 9 presents the resistance force of *AUV* hull vs. velocity. In addition, the required power of *AUV* hull is depicted vs. the range of velocity in Fig. 10.

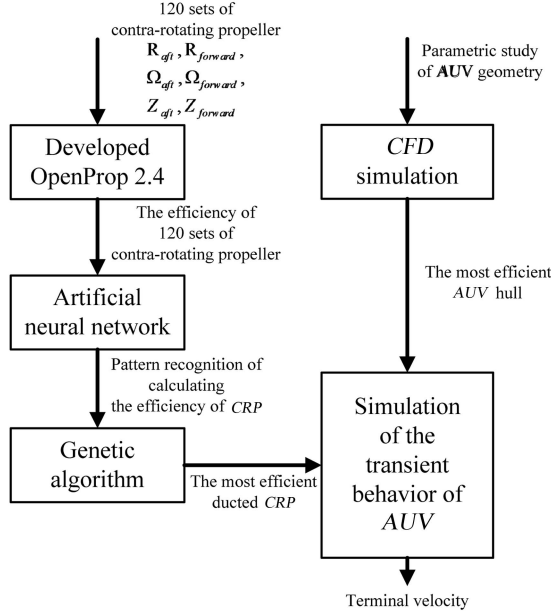


Fig. 11 comprehensive procedure of the most efficient AUV design

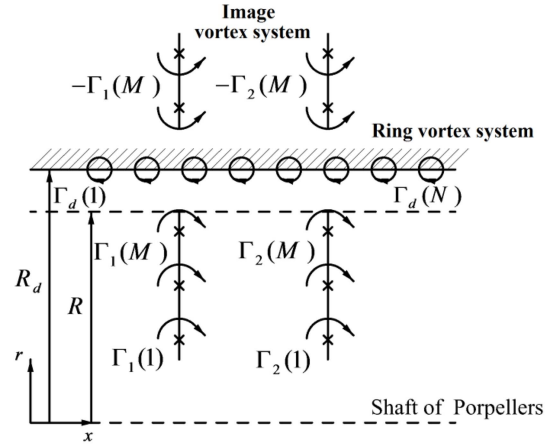


Fig. 12 the model of ducted CRP in lifting line theory

#### 4. The design of AUV propeller

The rotation torque in single propeller leads to the heel of the AUV hull fully submerged body. The implementation of contra-rotating propeller (CRP) is a remedy to cancel the torque of the propellers. Generally, the AUV hull is so sensitive to the noise due to embedding of the sonar system in the nose of the hull. So utilizing the duct around the propellers not only increases the thrust of propulsion system in low velocity but also reduces the noise of propellers

In the present work, the lattice vortex lifting line theory is applied to design DCRP. To reduce the computational time of propeller design, the genetic algorithm coupled with artificial neural network is applied to select the optimum DCRP. Figure 11 illustrates the procedure of DCRP in brief.

In the lifting line theory, each of the propellers is modeled by a lifting line theory involving some vortex point with unknown circulation. Besides, the duct is determined by some vortex points and a set of image vortex points to simulate the axial velocity close the wall duct. Figure 12 represents the circulation of the propellers and the duct in schematic.

To get the optimum design of DCRP, the delivered power as the objective function should be minimized for the constant desired thrust and AUV velocity. Moreover, the required thrust  $T_1 + T_2 + T_{duct} - F_{D,hub}$  as the first constraint should be totally provided by the set of the propellers and the duct and the torque ratio,  $q = Q_1 / Q_2$ , as the second constraint should be specified in the design. So the auxiliary function is defined by following equation

$$H = (Q_1 \omega_1 + Q_2 \omega_2) + \lambda_T (T_1 + T_2 + T_{duct} - F_{D,hub}) + \lambda_Q (Q_1 - q Q_2) \quad (19)$$

where  $\lambda_T$  and  $\lambda_Q$  are Lagrangian multipliers.

The torque and thrust of each propeller are determined as Coney formulation (Kerwin 1986, Stubblefield 2008). The duct thrust  $T_{duct}$  and drag force of duct  $F_{D,hub}$  in Eq. (19) are also attributed to the circulation on the vortex point along the duct (Matlab 2010) and effect of viscosity on the wall duct, respectively.

To determine the unknown circulations on the vortex points of aft and forward propellers, the partial derivatives of auxiliary function  $H$  should be zero respect to the unknown circulations and two Lagrangian multipliers as

$$\frac{\partial H}{\partial \Gamma_i} = 0, i = 1 \dots 2 M_p \quad \text{and} \quad \frac{\partial H}{\partial \lambda_T} = 0, \frac{\partial H}{\partial \lambda_Q} = 0 \quad (20)$$

An iterative algorithm is utilized to solve the nonlinear set of Eq. (20). Then genetic algorithm coupled with the artificial neural network is utilized to determine the fundamental variables of DCRP. The genetic algorithm (GA) mimics from the biological evolution based on the optimum natural selection. GA is used in the optimization of the constrained problems even with complex non-linearity (Kebriaee and Nasiri 2012).

In the first *generation* of GA, a *population* of some *individuals* are defined as candidates of solution by random or definite equation. Every member of the population is specified with a unique *chromosome* including a string of *genes*. Each individual of the current generation is scored by *fitness function*. After evaluating, the best members are chosen as *parents* to create the *offspring* of the next generation. Three main rules- elite, crossover and mutation- govern in the reproduction of the next generation. In the GA, each generation improves respect to the preceding generation and the average score of population evolves toward the optimum point.

The *artificial neural network* (ANN) is one of the most applicable tools in the *pattern recognition*. The ANN can be applied to predict the behavior of any non-linear complex system with transfer function. ANN involves one or more *layers* with two or more *neurons* interconnected by *synapse* network.

An adjustable *weight function* is attributed to any intermediate synapse, a fitting *bias function* is calculated for each layer, and a proper *transfer function* is defined for each neuron in ANN. The preliminary idea in ANN is to adjust both weight and bias functions during *train* process to describe the relation between input and *target* vectors. About 80% of input signals are used in the train process to calculate the desired weight and bias functions. About 10% of input signals are applied to validate the network, and the last 10% are used to the test of the network generalization, (Kebriaee and Nasiri 2012). The input signals of the present ANN are 120 contra-rotating propellers designed by lifting line theory. Each system has 6 independent variables as two diameters, two speed rotations, and two numbers of blades. Table 2 shows the performance of some samples of

Table 2. Some CRPs design by lifting line theory

	$R_1$	$R_2$	$Z_1$	$Z_2$	$N_1$	$N_2$	$\eta$
1	5.5	5	3	3	3750	4000	0.7320
2	4.75	5.25	4	3	6000	5500	0.6784
3	4.45	4.45	4	2	4600	4600	0.7086
4	5.05	5.05	2	3	4950	4950	0.6980

Table 3. Fundamental Variables of final *DCRP*

Propeller		Duct	
$R_1$	52.5 mm	$X_f$	28 mm
$R_2$	55 mm	$c_{duct}$	80 mm
$Z_1$	4	Meanline	<i>NACA66</i>
$Z_2$	4	Thickness	<i>NACA a = 0.8</i>
$N_1$	3500 RPM		
$N_2$	3500 RPM		
Meanline	<i>NACA66</i>		
Thickness	<i>NACAA = 0.8</i>		

*DCRP*. As the number of input signals also is not enough in one training process, the present *ANN* is trained about 25 times with the invariant inputs. Finally, *GA* with fitness function of *ANN* was applied to determine the optimum *CRP*.

The best propeller was introduced by *GA* in the 51<sup>th</sup> generation. Table 3 illustrates the fundamental variables of the most optimum ducted *CRP* determined by *GA*. As the final result, Fig. 13 depicts the 3D design of *DCRP*. More details about *DCRP* design can be studied in (Drela 2007).

## 5. Selection of AUV electrical motor

The first point to select the electrical motor is attributed to battery specifications. As the maximum *AUV* operation time is about 5 minutes, the upper bound of motor current will be less than 60 A.

The behavior of electrical motor is prescribed by an *equivalent electrical circuit*, Fig. 14.

The required electrical current,  $I$ , for certain angular velocity,  $\Omega$ , is attributed to a practical coefficient called as the *motor speed constant*,  $K_{v_m}$ , and determine by

$$I = (v - \Omega / K_{v_m}) / R \quad (21)$$

where  $v$  is the terminal voltage of the battery and  $R$  is the internal resistance. The motor torque  $Q_m$  is also defined as (Drela 2007).

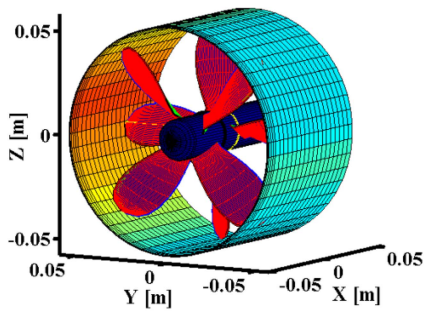
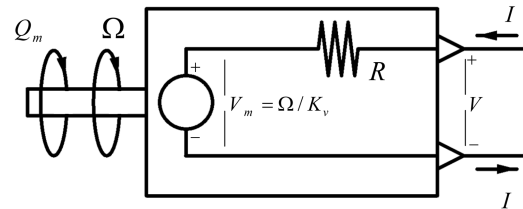
Fig. 13 3D *DCRP*

Fig. 14 Equivalent circuit of motor

Table 4 The specification of the brushless electrical motor

Motor Specification	Value
<i>RPM/V</i>	170
Max Efficiency current	36-84 (>85%)
No load current	2.1 A
Internal resistance	26 mOhem

$$Q_m = \frac{(I - I_o)}{K_{Q_m}} \quad (22)$$

The motor torque constant can be expressed by

$$K_{Q_m} = \frac{K_{V_m} \times 60}{2\pi} \quad (23)$$

$I_o$  is also the no-load current of motor in Eq. (22). After determining terminal current, voltage, torque, and rotation of motor can be calculated via Eqs. (20)-(23). The delivered motor torque is to fix with torque of *DCRP*. In addition, motor and *DCRP* should be synchronized by the same angular velocity. Table 4 reports the specifications of final electrical motor. The rotation rate, torque, and output power are about 3500RPM, 2.1 N.m, and 770 W, respectively for 22.2 v and 40A battery terminal voltage and current in the maximum *AUV* operation time.

### 6. Simulation of *AUV* motion

The behavior of *AUV* system including *AUV* hull, propeller, and electrical motor should be evaluated as a unique system based on modeling of each component.

Fig. 15 illustrate interconnection between different components of *AUV* in schematic. As seen, the

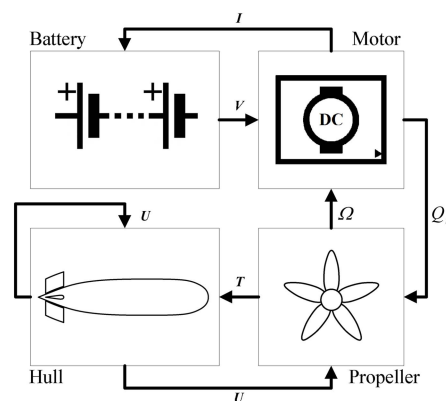


Fig. 15. schematic of *AUV* simulation

battery provides a certain voltage for the brushless electrical motor and the electrical motor determines the battery current as

$$I_{motor} = \left( v - \frac{\Omega}{K_{v_{motor}}} \right) \frac{1}{R} \quad (24)$$

In addition, the electrical motor delivers a specific rotation torque to the propeller based on Eq. (22) and the propeller translates the angular velocity to the electrical motor with an interconnected shaft. The angular velocity of the propeller is calculated by integrating from angular acceleration,  $\bar{\alpha}$ , defined as

$$(I_{1,2} + I_{motor})\bar{\alpha} = Q_{motor} - Q_1 - Q_2 \quad (25)$$

To determine the propellers torque,  $Q_1$  and  $Q_2$ , the torque coefficient of each propeller,  $K_{Q1}$  and  $K_{Q2}$ , is calculated as a function of geometry and advanced velocity expressed by

$$J = V / (nD_{1,2}) \quad (26)$$

where  $n$  is the angular velocity in *RPS* and  $V$  is the velocity close to the propellers and  $D_1$  and  $D_2$  are the propellers diameter.

The torque of the propellers is obtained by

$$Q_{1,2} = K_{Q_{1,2}} \rho n_{1,2}^2 D_{1,2}^5 \quad (27)$$

The *DCRP* generates the required thrust of the hull by following equation,

$$T_{1,2} = K_{T_{1,2}} \rho n_{1,2}^2 D_{1,2}^4 \quad (28)$$

Also the thrust of the duct  $T_D$  is appended to the propellers thrust.

Finally, the acceleration of *AUV* system ( $a$ ) is determined to find the maximum velocity in the straight path, as the design target, as follows

$$(m_{hull} + m_{added})a = (T_1 + T_2 + T_D - F_{D_{hull}}) \quad (29)$$

where the drag of hull is calculated from Fig. 9.

The mass of *AUV* is also 12.2 kg and  $m_{added}$  is the added mass defined as

$$m_{added} = 0.818 \rho \pi r_{hull}^2 L_{hull} \quad (30)$$

## 7. Results of simulation

After selecting the optimum hull and motor as well as designing the *DCRP*, Eqs. (21)-(30) are applied to simulate the motion of *AUV*. Figure 16 illustrates the transient behavior of *AUV* hull in the first 25 seconds. Results also show *AUV* can achieve to the maximum velocity, 24 knots, after

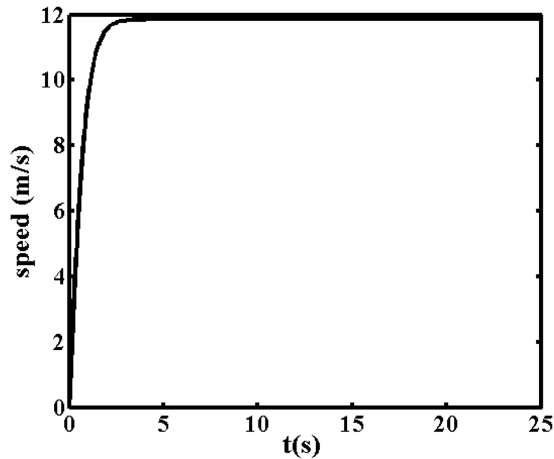


Fig. 16. velocity of AUV hull vs. time

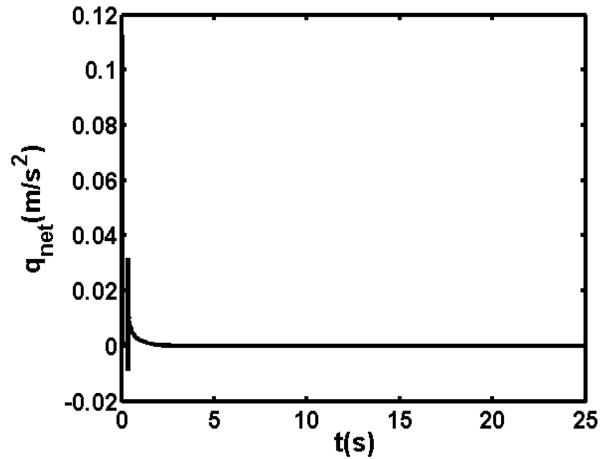


Fig. 17. net of applied torque on the hull vs. time

less than 5 seconds. In addition, Fig. 17 illustrates no net torque applied to the hull by the set of *DCRP* expect in the very early seconds.

This design methodology was applied to determine the design variables of Arsin AUV. In the early experiments, the results represented the maximum velocity of AUV was about 21 knot. In addition, the net torque of the propellers regardless of this high velocity equals zero and no heel was observed in the dynamic motion of AUV.

## 8. Conclusions

In the present work, the procedure of mechanical design of AUV was described in detail. The mechanical design of AUV is categorized in three parts of hull design, propeller design, and electrical motor selection. Applying the *CFD* tools, the optimum hull was determined with minimum resistance drag. Results illustrated the profile of *NACA0014* is the best option for the hull nose. Then the lifting line theory was applied to design the ducted contra-rotating propellers. To reduce the design time, the genetic algorithm coupled with artificial neural network was utilized to select the best *DCRP*. So the 4-blade propellers with 10.5 and 11 cm diameter were selected as the best propellers. The selection of electrical motor was also based on the first order model of electrical motors. Interconnecting the performance of each mechanical component caused to get the optimum AUV with high velocity. The result of simulation showed the maximum velocity of AUV is about 24 knots and no rotation torque is applied on the hull by using the ducted contra-rotating propellers.

## References

- Alemayehu, D., Boyle, R.B., Eaton, E., Lynch, T., Stepanchick, J. and Yon, R. (2006), *Design report guided missile submarine SSG(X)*, Ocean Engineering Design Project AOE 4065/4066.
- Alvarez, A., Bertram, V. and Gualdesi, L. (2009), "Hull hydrodynamic optimization of autonomous underwater

- vehicles operating at snorkeling depth”, *Ocean Eng.*, **36**(1). 105-112.
- Bertram, V. and Alvarez, A. (2006), “Hydrodynamic aspects of AUV design”, *Proceedings of the 5th Conference on Computer and IT Applications in the Maritime Industries (COMPIT)*, Oegstgeest, Netherlands.
- Brown, A. and Thomas, M. (1998), *Reengineering the naval ship concept design process*, ASNE from Research to Reality in Ship systems Engineering Symposium, Tysons Corner, VA, September.
- Chen, Y. (1999), *Formulation of a multi-disciplinary design optimization of containerhips*, MS Thesis, Department of Aerospace and Ocean Engineering, Virginia. Stepanchick, J. and Brown, A. (2006), “Revisiting DDGX/DDG-51 Concept Exploration”, ASNE Day, Arlington, VA, June.
- Coney, W. (1989), *A method for the design of a class of optimum marine propulsors*, Ph. D. Thesis, Cambridge, MA: Massachusetts Institute of Technology.
- De Barros, E.A., Dantas, J.L.D., Pascoal, A.M. and De Sá, E. (2008), “Investigation of normal force and moment coefficients for an AUV at nonlinear angle of attack and sideslip range”, *IEEE J. Oceanic Eng.*, **33**(4), 538-549.
- Drela, M. (2007), *First-order DC electric motor model*, MIT Aero & Astro.
- Epps, B.P. (2010), *Openprop v2.4 theory document*, MIT Department of Mechanical Engineering Technical Report.
- Good, N. and Brown, A. (2006), *Multiple-objective concept design of an advanced logistics delivery system ship (ALDV)*, ASNE Joint Sea Basing Symposium, Arlington, VA, March.
- Joubert, P.N. (2006), *Some aspects of submarine design Part 2: shape of a submarine 2026*, Technical Report, DSTO-TR-1920, December.
- Joung, T., Sammut, K. He, F. and Lee, S.K. (2009), “A Study on the design optimization of an AUV by using computational fluid dynamic analysis”, *Proceedings of the 19th International Offshore and Polar Engineering Conference Osaka*, Japan, June 21-26.
- Kebriaee A. and Nasiri H. (2012), “Optimum design and simulation of ducted contra-rotating propellers with lifting-line theory, neural network, and genetic algorithm”, submitted in *Applied Ocean Research Journal*.
- Keller, J. aufm (1966), *Enige aspecten bij het ontwerpen van scheepsschroeven*, Schip en Werf, No. 24.
- Kerwin, J., Coney, W. and Hsin, C. (1986), *Optimum circulation distributions for single and multi- components propulsors*, 21st American Towing Tang Conference, Washington DC, National Academy press.
- Lutz, T. and Wagner, S. (1998), “Numerical shape optimization of natural laminar flow bodies”, *Proceedings of the 21st ICAS Congress*, Melbourne, Australia.
- Mackay, M. (2003), *The standard submarine model: a survey of static hydrodynamic experiments and semiempirical predictions*”, Technical Report DRDC Atlantic TR 2003-079, June.
- Martz, M.A. (2008), *Preliminary design of an autonomous underwater vehicle using a multiple-objective genetic optimizer*, Master’s thesis, Virginia Polytechnic Institute and State University, Blacksburg, Virginia, United States, May.
- Matlab 2010 Documentation (2010), The MathWorks, Inc.
- Michel, R. (1951), *Etude de la transition sur les profile d’ aile; Etablissement d’un critere de determination de point de transition et calcul de la trainee de profile incompressible*, ONERA Report 1/1578A, 1951.
- Phillips, A.B., Turnock, S.R. and Furlong, M. (2010), “The use of computational fluid dynamics to aid cost-effective hydrodynamic design of autonomous underwater vehicles”, *Proceedings of the Institution of Mechanical Engineers, Part M: J. Engineering for the Maritime Environment*.
- Shome, S.N., Nandy, S., Das, S.K., Biswas D.K. and Pal, D. (2008), “AUV for shallow water applications – some design aspects”, *Proceedings of the 18th International Offshore and Polar Engineering Conference Vancouver*, BC, Canada, July 6-11.
- Stubblefield J.M. (2008), *Numerically based ducted propeller design using vortex lattice lifting line theory*, Ms. Thesis, Cambridge, MA.

**Nomenclatures**

$D$	Diameter	$Re$	Reynolds number	<b>Greek</b>	
$F_D$	drag force	$S$	wetted surface	$\Gamma$	Circulation on control point
$i$	terminal current	$t$	thrust reduction coefficient	$\eta$	efficiency
$i_o$	no-load current	$T$	Thrust	$\theta$	momentum thickness
$K_Q$	torque constant	$u$	Velocity	$\rho$	Density
$K_V$	speed & thrust constant	$v$	terminal voltage	$\mu$	viscosity coefficient
$L$	Length	$V$	velocity magnitude	$\Omega$	rotation rate
$P$	Pressure	$w$	wake coefficient	<b>Subscripts</b>	
$Q$	Torque	$x$	distance along the hull	1,2	forward and aft propeller
$r$	Radius	$z$	blade number	$m$	Motor
$R$	internal resistance			$p$	propeller
				$r, \theta, z$	Cartesian coordinate